

Modeling Infrastructure Degradation from Visual Inspections Using Network-Scale State-Space Models

ZACHARY HAMIDA*and JAMES-A. GOULET
Department of Civil, Geologic and Mining Engineering
POLYTECHNIQUE MONTREAL, CANADA

March 29, 2020

Abstract

Visual inspections is a common approach for the network-scale monitoring of bridges. One of the main challenges when interpreting visual inspections is the observations being subjective and thus the observation uncertainty varies among different inspectors. In addition, observations uncertainties can be dependent on the structural element condition. These two factors introduce difficulties in differentiating between measurement errors and legitimate changes in a structure's condition. This study proposes a state-space model suited for the network-scale analyses of transportation infrastructure. The formulation of the proposed framework enables quantifying the uncertainty associated with each inspector. In addition, the proposed model accounts for the uncertainty of visual inspections based on the structure condition as well as the uncertainty specific to each inspector. The predictive capacity and robustness of the proposed model is verified with synthetic inspection data, where the true deterioration state is known. Following the verification step, the proposed model is validated with real data taken from a visual inspections database.

Keywords: Visual Inspections, Inspector Uncertainty, Bridge Network, State-Space Models, Structural Health Monitoring.

1 Introduction

The aging of transportation infrastructure has increased the demand for data-driven asset management. Monitoring bridges through visual inspections is a common practice among many infrastructures management agencies [24, 34, 23, 9]. The popularity of visual inspections can be attributed to the advantage of providing direct information about the health of structures. These information are based on a broad evaluation which does not target a specific type of damage or a structural component [1]. Although visual inspections is a common monitoring approach, along with many advantages, it suffers from shortages that limit its efficiency. Visual inspections are performed by different individuals over time, therefore, it is common to have inconsistencies in the recorded data [1, 35, 26, 5]. These inconsistencies introduce difficulties in differentiating between measurement errors and legitimate changes in a structure's condition. Therefore, it becomes challenging to accurately model the deterioration behaviour.

Many studies have adopted *discrete Markov models* (DMM) for modeling the deterioration behaviour based on visual inspections [34, 17, 18, 15, 11, 13, 36, 40]. While DMM-based models are easy to implement, relying on this type of models is subject to inherent limitations that affect the deterioration model's overall performance. One of the common limitations in existing deterioration models is omitting the inspector uncertainty from the model. Several studies have described the inspector uncertainty as one of the main sources of variability in visual inspection data [1, 24, 4]. Current DMM models have accommodated the *epistemic* uncertainty and the *aleatory* uncertainty in the inspection data [40]; However, the inspectors uncertainty is typically overlooked. Theoretically, the inspector uncertainty can be estimated in a *Hidden Markov Model* (HMM) [29] with an *observation matrix* for

*Corresponding author: zachary.hamida@polymtl.ca

each inspector. However, in practice, given the large number of inspectors, estimating an *observation matrix* for each inspector is seldom feasible. This is because the amount of data required for the model parameters estimation is unattainably large, in addition to being computationally expensive. Another limitation in the DMM models is attributed to the discretization aspect. Relying on discrete states in representing a naturally continuous physical process can introduce approximation errors. These approximation errors can result in additional flaws in forecasting the deterioration process [7]. In addition, the speed of deterioration over time can not be directly quantified, as quantifying the speed requires representing the deterioration by a continuous process. The importance of quantifying the speed of deterioration arise from the prospect of enabling further analysis such as modeling the effect of interventions. Further factors that add up to the limitations in Markov models are the stationarity of the transition probabilities, the duration independence and the interpretability which are detailed in the work of Zambon et al. [38]. Recent studies have addressed the stationarity and discretization issues by using a semi-Markov process model [25, 27, 39], however, this type of Markov models may require having an analytical deterioration model to enhance its performance [38].

Another perspective on modeling the deterioration behaviour in infrastructures is by employing regression models in analyzing time series data. Various regression techniques are applied to structural health monitoring problems [10, 8]. However, within the confines of visual inspections data, the use of regression models is found to be limited in the literature [37, 14, 20]. This is due to some of the characteristics in the visual inspection data. For example, in analyses on short time series, it is challenging for a regression model to capture the temporal dependence in the time series and provide reliable predictions [22, 12]. In addition, the processes of training and validating a regression model are typically offline. Thus, at any point in time, if a new data becomes available, it is required to repeat the training and the validation of the deterioration model. Other factors that can impact the performance of regression models are the imbalanced representation of the system response and the quality of the regression covariates [21]. These factors may impose additional challenges when working with regression models.

This study propose a new method that is based on *state-space models* and that is suited for network-scale analyses of transportation infrastructures. The core objective of this model is to forecast the deterioration of different structural elements over time, along with quantifying the speed of deterioration. In the proposed framework, the uncertainty associated with each inspector is quantified based on the inspection data from the bridges network. In addition, the inspection uncertainty is considered dependent on the structural element deterioration state as well as the inspector’s uncertainty. The outcome of the study is a general data analysis framework that will help monitoring and maintaining existing infrastructure by enabling tracking the performance of structural elements, forecasting the deterioration and assessing the deterioration rate. The prediction capacity of the model is verified with synthetic data and validated with real data acquired from a Canadian bridge network.

2 Methodology

This section describes the proposed framework for modeling the deterioration behaviour and quantifying visual inspections uncertainty.

2.1 Context & Notations

The hierarchy of visual inspection data can be subdivided into three levels: the *network level*, the *bridge level* and the *element level*. The *network level* defines the transportation network regional properties (i.e. inspection code, country, . . . , etc.). Following the *network level*, is the *bridge level* defined by the set of bridges $\mathcal{B} = \{b_1, b_2, \dots, b_B\}$. The last level is the *element level* defined by the set of structural elements $\mathcal{E} = \{e_1^j, e_2^j, \dots, e_{E_j}^j\} \subset \mathcal{B}$. The deterioration information collected through inspections are added to the hierarchy at the *element level*. These information include the inspection time t , the engineer I_i from the group of inspectors $\mathcal{I} = \{I_1, I_2, \dots, I_I\}$ responsible for evaluating the bridges in \mathcal{B} and the condition of the structural element $\tilde{y} \in [l, u]$. The domain $[l, u]$ represent the range of values in which an inspector can assign to a structural element, with u representing the best health condition and l is the worst health condition. The symbol (\sim) in \tilde{y} is utilized to differentiate

between observations in the bounded space $[l, u]$ and unbounded space \mathbb{R} which is further detailed in Section 2.3.2.

2.2 State-Space Model

State-space models (SSM) are well suited for time series data and allow estimating the hidden states of a system from imperfect observations. The term hidden states refers to the unobservable states of the system. A state-space model is composed of two models: an *observation model* and a *transition model*. The formulas describing each model are,

$$\overbrace{\mathbf{y}_t = \mathbf{C}\mathbf{x}_t + \mathbf{v}_t}^{\text{observation model}}, \underbrace{\mathbf{v}_t : \mathbf{V} \sim \mathcal{N}(\mathbf{v}; \mathbf{0}, \mathbf{R}_t)}_{\text{observation errors}} \quad (1)$$

$$\overbrace{\mathbf{x}_t = \mathbf{A}\mathbf{x}_{t-1} + \mathbf{w}_t}^{\text{transition model}}, \underbrace{\mathbf{w}_t : \mathbf{W} \sim \mathcal{N}(\mathbf{w}; \mathbf{0}, \mathbf{Q}_t)}_{\text{process errors}} \quad (2)$$

where \mathbf{y}_t represents the observations, \mathbf{C} is the observation matrix, \mathbf{x}_t is the state vector at time t : $\mathbf{x}_t : \mathbf{X} \sim \mathcal{N}(\mathbf{x}, \boldsymbol{\mu}_t, \boldsymbol{\Sigma}_t)$, \mathbf{A} is the state transition matrix, \mathbf{v}_t , \mathbf{w}_t are the observation and process errors and \mathbf{R}_t , \mathbf{Q}_t represent respectively the observations and transition error covariance matrices. Different algorithms for estimating hidden states exist in the literature for different types of problems [6, 19, 16]. In this study, the estimation of the hidden states is done through the *Kalman filter* (KF) [19] expressed in the short form as,

$$(\boldsymbol{\mu}_{t|t}, \boldsymbol{\Sigma}_{t|t}, \mathcal{L}_t) = \text{Kalman filter}(\boldsymbol{\mu}_{t-1|t-1}, \boldsymbol{\Sigma}_{t-1|t-1}, \mathbf{y}_t, \mathbf{A}_t, \mathbf{Q}_t, \mathbf{C}_t, \mathbf{R}_t), \quad (3)$$

where \mathcal{L}_t represent the log-likelihood for observation \mathbf{y}_t , $\boldsymbol{\mu}_{t|t} \equiv \mathbb{E}[\mathbf{X}_t | \mathbf{y}_{1:t}]$ the posterior expected value and $\boldsymbol{\Sigma}_{t|t} \equiv \text{cov}[\mathbf{X}_t | \mathbf{y}_{1:t}]$ the posterior covariance at time t respectively, given observations $\mathbf{y}_{1:t}$. In addition to KF, the *Kalman smoother* (KS) [30] is utilized to propagate the knowledge acquired from later observations onto previous hidden states.

In some applications, it is required to constrain the state estimates of the state-space models. This is to prevent the model from providing or relying on state estimates that are incompatible with the physics of the problem. Different approaches are described in the literature for imposing constraints in the KF framework [32, 33]. In this study, the PDF truncation method [33] is utilized for handling the deterioration model constraints. The PDF truncation method relies on the concept of truncating the PDF of the states at the constraint bounds. Thereafter, the truncated area within the feasible bounds is approximated by a *Normal* PDF representing the constrained state estimate.

2.3 Quantifying Visual Inspections Uncertainty

This section presents the proposed framework for quantifying the uncertainty associated with visual inspection data.

2.3.1 Inspector-Dependent Uncertainty

Visual inspections are performed by different individuals $I_i \in \mathcal{I} = \{I_1, I_2, \dots, I_I\}$ over time, therefore, it is common to observe variability in the recorded data [31, 4, 2]. This variability is mainly attributed to the subjective nature of the evaluation. The variability in the observations is commonly quantified in state-space models through estimating a single standard deviation parameter σ_V common for all observations such that, for any structural element e_k^j in bridge b_j , the observation error $v_{t,k}^j : V \sim \mathcal{N}(v; 0, \sigma_V^2)$. Here, in order to account for the inspectors uncertainty, each inspector I_i is assigned a standard deviation parameter $\sigma_V(I_i)$. The standard deviations $\sigma_V(I_i)$ are considered as model parameters to be estimated from the data as detailed in Section 2.5.1. Such formulation allows characterizing inconsistencies that may exist in a sequence of observations obtained from different inspectors.

2.3.2 State-Dependant Uncertainty

In addition to considering the uncertainty $\sigma_V(I_i)$ as a function of the inspector, it is required to take into account that inspection uncertainty can also be dependant on the structural element's condition [4]. For example, if the structural element $e_k^j \in \mathcal{B}$ is in a perfect condition ($\tilde{x}_k^j = u$), then an inspector I_i is less likely to misjudge its condition. Similarly for structural elements with a poor condition ($\tilde{x}_k^j = l$). On the other hand, for structural elements with a partial damage (e.g. $\tilde{x}_k^j = \frac{l+u}{2}$), the prospect of misjudging the structural element condition becomes higher. In order to accommodate the aforementioned uncertainty characteristics, non-linear space transformation is applied on the data. Space transformation is done by using a transformation function that maps each point from the original space to a point in the transformed space (i.e. $g : [l, u] \rightarrow \mathbb{R}$). Applying a proper transformation in this context allows the observation and transition uncertainty to become a function of the structural element's deterioration state \tilde{x} . In addition, space transformation can enable constraining the deterioration state estimate \tilde{x} within the feasible interval of the deterioration condition $[l, u]$. To attain both of the aforementioned properties, a step function with special characteristics is proposed. These characteristics are: a linear middle span with 1 : 1 slope ratio (i.e. $\frac{dx}{d\tilde{x}} = 1$) and non-linear ends, and for which the first derivative is known. A transformation function that fulfill the desired characteristics, along with its inverse, is described by,

$$x = g(\tilde{x}) = \begin{cases} \left[\frac{1}{\Gamma(\alpha)} \int_0^{\tilde{x}} t^{\alpha-1} e^{-t} dt \right]^\alpha, & \frac{u+l}{2} < \tilde{x} \leq u, \\ \tilde{x}, & \tilde{x} = \frac{u+l}{2}, \\ - \left[\frac{1}{\Gamma(\alpha)} \int_0^{\tilde{x}} t^{\alpha-1} e^{-t} dt \right]^\alpha, & l \leq \tilde{x} < \frac{u+l}{2}, \end{cases} \quad \tilde{x} = g^{-1}(x) = \begin{cases} \frac{1}{\Gamma(\alpha)} \int_0^{x^{\frac{1}{\alpha}}} t^{\alpha-1} e^{-t} dt, & x > \frac{u+l}{2}, \\ x, & x = \frac{u+l}{2}, \\ - \frac{1}{\Gamma(\alpha)} \int_0^{x^{\frac{1}{\alpha}}} t^{\alpha-1} e^{-t} dt, & x < \frac{u+l}{2}. \end{cases} \quad (4)$$

The function $g(\tilde{x})$ maps a deterioration state $\tilde{x} \in [l, u]$, labelled as the original space, to $x \in [-\infty, \infty]$ labelled as the transformed space. From Equation 4, the parameter α is given by: $\alpha = 2^{-n}$, where n is a positive integer $n \in \mathbb{Z}^+$. The role of the parameter n is to control the curvature at the transformation function ends. Figure 1 illustrates the transformation function $g(\tilde{x})$ with different n values. For $n = 1$, the transformation function has a low curvature. As the parameter n value increases, the curvature becomes higher. However, for all n , the slope ratio remains fixed at 1 : 1 for the middle span. Moreover, it is noted that for $n \geq 4$, the change in the shape of the transformation function is insignificant in which $n = 5$ is roughly equivalent to a linear transformation. Therefore, the possible values for the parameter n can be limited to $n \in \{1, 2, 3, 4, 5\}$. Identifying the parameter n that best suit the problem context is done through the parameter estimation framework described in section 2.5.1.

In order to demonstrate the role of the transformation function, Figure 2 presents two examples for the application of space transformation using the function $g^{-1}(x)$ in Equation 4 on a Normal PDF defined in $x \in [-\infty, \infty]$. The first example is demonstrated with the dashed-line PDFs in Figure 2a and 2b.

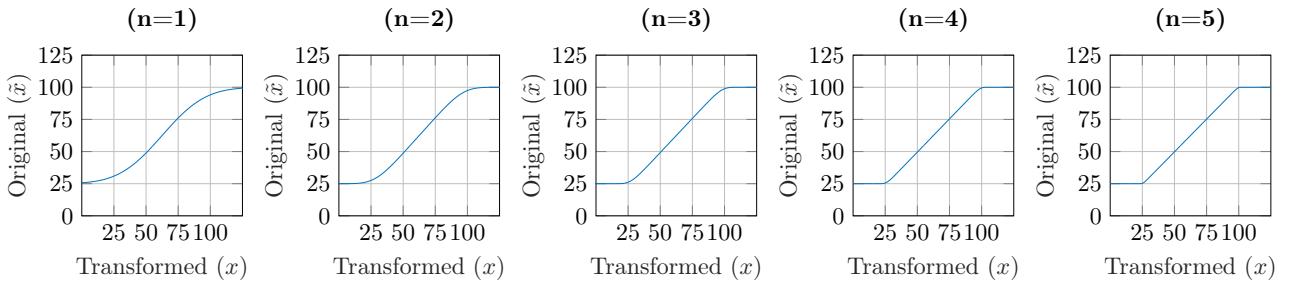


Figure 1: Transformation function $g(\cdot)$ with different n values.

This example illustrates how the probability content is adjusted when the expected value of the state in the unbounded space ($x \in [-\infty, \infty]$) has a value near the lower bound $l = 25$ of the bounded space ($\tilde{x} \in [25, 100]$). On the other hand, the second example demonstrated with the continuous-line PDFs in Figure 2a and 2b, shows that when the expected value of the state is closer to the middle span, the PDF in the bounded space reflects subtle differences from the PDF in the unbounded space. In summary, the

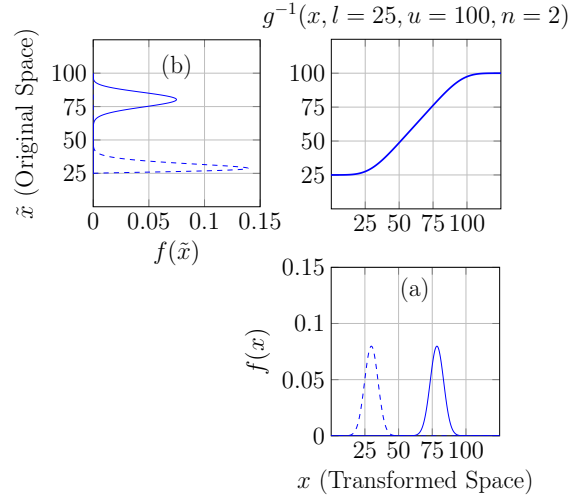


Figure 2: Examples of state transformation with the proposed transformation function.

purpose of introducing the transformation function $g(\cdot)$ is to enable the inspections uncertainty to be dependent on the deterioration state of the structural element and restrict the estimated deterioration state within the feasible deterioration condition bounds $[l, u]$.

2.4 Deterioration Model Constraints

The uncertainty and insufficiency of the inspection data for each bridge may result in unrealistic trends in the time series data of the structural elements. For example, a set of observations may wrongfully indicate that an element's condition is improving over time without interventions being made on the structure. In order to prevent such a problem, constraints are applied for each time step. The constraint ensures that the deterioration condition between any consecutive time steps t and $t + 1$ is not improving. This is achieved by constraining the speed to be negative through the following criterion: $\dot{\mu} + 2\sigma^{\dot{x}} \leq 0$, with $\dot{\mu}$ and $\sigma^{\dot{x}}$ are respectively the expected value and the standard deviation of the speed \dot{x} . The PDF truncation method [33] is employed if the aforementioned constraint is violated in the proposed model.

2.5 Deterioration Model

The proposed framework for modeling the deterioration process in structural elements is based on state-space models. The goal of this framework is to model the deterioration behaviour with a *kinematic model* [3], that includes the element condition x , degradation speed \dot{x} and acceleration \ddot{x} as defined by,

$$\underbrace{\begin{bmatrix} x_t \\ \dot{x}_t \\ \ddot{x}_t \end{bmatrix}}_{\mathbf{x}_t} = \underbrace{\begin{bmatrix} 1 & \Delta t & \frac{\Delta t^2}{2} \\ 0 & 1 & \Delta t \\ 0 & 0 & 1 \end{bmatrix}}_{\mathbf{A}} \cdot \underbrace{\begin{bmatrix} x_{t-1} \\ \dot{x}_{t-1} \\ \ddot{x}_{t-1} \end{bmatrix}}_{\mathbf{x}_{t-1}} + \underbrace{\begin{bmatrix} w_t \\ \dot{w}_t \\ \ddot{w}_t \end{bmatrix}}_{\mathbf{w}_t}, \quad (5)$$

where \mathbf{x}_t and \mathbf{x}_{t-1} are the state vector at time t and $t - 1$, \mathbf{A} describes the model kinematics for transitioning from \mathbf{x}_{t-1} to \mathbf{x}_t and \mathbf{w}_t is the model-error vector. The kinematic model in Equation 5 is employed within the proposed framework to characterize the degradation behaviour in bridges \mathcal{B} . Therefore, for each structural element $e_k^j \in \mathcal{E} \subset \mathcal{B}$, the *transition model* that describes the deterioration process from time $t - 1$ to time t is,

$$\mathbf{x}_{t,k}^j = \mathbf{A}\mathbf{x}_{t-1,k}^j + \mathbf{w}_t, \quad (6)$$

where $\mathbf{x}_{t,k}^j$ is the state vector at time t consisting of the condition $x_{t,k}^j$, the speed of degradation $\dot{x}_{t,k}^j$ and the acceleration $\ddot{x}_{t,k}^j$. The expected value of each component in the state vector $\mathbf{x}_{t,k}^j$ is represented by $\mu_{t,k}^j$ for the condition, $\dot{\mu}_{t,k}^j$ for the speed and $\ddot{\mu}_{t,k}^j$ for the acceleration. The matrix \mathbf{A} in the transition

model represents the transition matrix and $\mathbf{w}_t : \mathbf{W} \sim \mathcal{N}(\mathbf{w}; \mathbf{0}, \mathbf{Q}_t)$ represents the model-error vector with the model error covariance [3] \mathbf{Q}_t defined by,

$$\mathbf{Q}_t = \sigma_W^2 \times \begin{bmatrix} \frac{dt^5}{20} & \frac{dt^4}{8} & \frac{dt^3}{6} \\ \frac{dt^4}{8} & \frac{dt^3}{3} & \frac{dt^2}{2} \\ \frac{dt^3}{6} & \frac{dt^2}{2} & dt \end{bmatrix}.$$

The observation model for this SSM is described by,

$$\mathbf{y}_{t,k}^j = \mathbf{C}\mathbf{x}_{t,k}^j + v_{t,k}^j, \quad (7)$$

where $\mathbf{y}_{t,k}^j$ is the observation in the transformed space, \mathbf{C} is the observation matrix defined by $\mathbf{C} = [1 \ 0 \ 0]$ and $v_{t,k}^j : V \sim \mathcal{N}(v; 0, \sigma_V^2(I_i))$ is the observation error with $\sigma_V(I_i)$ being the standard deviation of the error associated with the observations of an inspector $I_i \in \mathcal{I}$. Figure 3 illustrates the details and the steps of the proposed degradation model for predicting and forecasting the deterioration behaviour of a single structural element e_k^j from time t up to time T . In this context, time T represents the time step associated with the last inspection point.

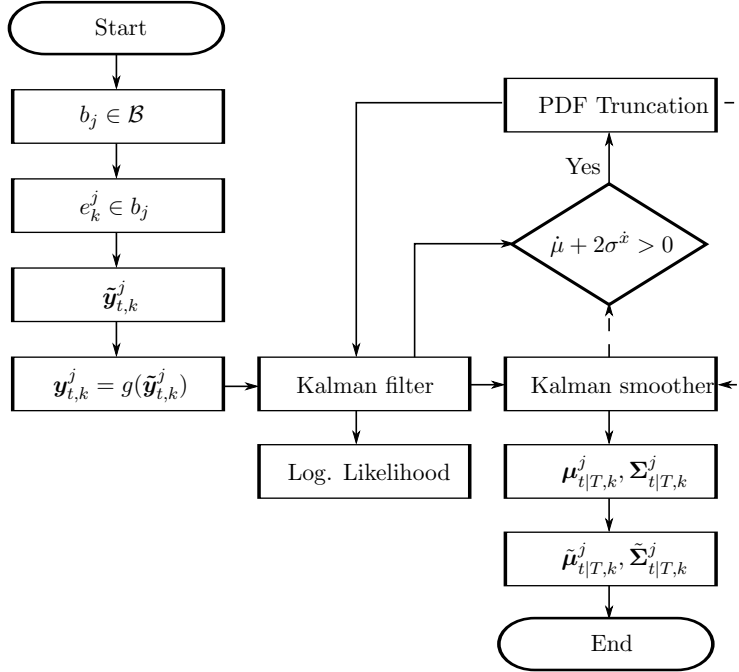


Figure 3: Structural degradation model for predicting and forecasting the deterioration state of structural element e_k^j from time t to time T .

The framework starts with the observation $\tilde{y}_{t,k}^j \in [l, u]$ representing the condition of structural element $e_k^j \in \mathcal{E} \subset \mathcal{B}$. The observation $\tilde{y}_{t,k}^j$ is passed in the transformation function $g(\cdot)$ presented in Equation 4 to obtain the transformed state observation $\mathbf{y}_{t,k}^j \in \mathbb{R}$. Following the transformation step, the observations are ready for the time series analysis through the Kalman filter and smoother. For any time series data $\mathbf{y}_{t,k}^j$, the Kalman filter starts at time $t = 0$ with an initial estimate for the state expected value vector $\boldsymbol{\mu}_{0,k}^j = [\mu_{0,k}^j \ \dot{\mu}_{0,k}^j \ \ddot{\mu}_{0,k}^j]^\top$ and the covariance matrix $\boldsymbol{\Sigma}_{0,k}^j = \text{diag} [\sigma_{0,k}^{x,j} \ \sigma_{0,k}^{\dot{x},j} \ \sigma_{0,k}^{\ddot{x},j}]^2$. In the covariance matrix, the variance of the initial speed is described by the function,

$$(\sigma_0^{\dot{x}})^2 = p_1^2(u - \tilde{\mu}_{c,1}) + p_2^2, \quad (8)$$

where p_1, p_2 are model parameters to be estimated from the inspection data and $\tilde{\mu}_{c,1}$ is the expected value of the condition at time $t = 1$. Initially $\tilde{\mu}_{c,1}$ is considered equal to the first observation $\tilde{\mu}_{c,1} = \tilde{y}_1$,

however, after obtaining the smoothed states, $\tilde{\mu}_{c,1}$ is set equal to the expected value of the smoothed state $\tilde{\mu}_{c,1} = \tilde{\mu}_{1|T}$. Equation 8 is employed to facilitate the estimation of the initial speed, given that few observations are available in each time series. Furthermore, the initial estimate for the expected condition $\mu_{0,k}^j$ is assumed to be equal to the average of the first three observations, while the initial expected speed and acceleration are considered as $\dot{\mu}_{0,k}^j = \ddot{\mu}_{0,k}^j = 0$. The initial state $\boldsymbol{\mu}_{0,k}^j, \boldsymbol{\Sigma}_{0,k}^j$ is propagated in time using the *prediction step* and the *update step* of the Kalman filter. After each update step, the constraint $\dot{\mu}_{t|t,k}^j + 2\sigma_{t|t,k}^{\dot{x},j} \leq 0$ is examined (see Section 2.4). If the aforementioned constraint is violated, the PDF truncation method is employed to constrain the estimate of the speed $\dot{x}_{t|t,k}^j$ within the feasible bounds. Following the filtering step, the Kalman smoother is utilized to refine the state estimates and the initial state at time $t = 0$. Because the number of observations $\mathbf{y}_{t,k}^j$ is limited per structural element, the refined estimate for the initial state $\mathbf{x}_{0,k}^j$ can be further improved in the parameter estimation framework described in the next section. After the smoothing step, the outputs $\boldsymbol{\mu}_{t|T,k}^j, \boldsymbol{\Sigma}_{t|T,k}^j$ are back-transformed to the original space $\tilde{\boldsymbol{\mu}}_{t|T,k}^j, \tilde{\boldsymbol{\Sigma}}_{t|T,k}^j$ for interpretation and analysis. This back-transformation step is done using the inverse transformation function $g^{-1}(\cdot)$ described in Equation 4. The next section describes the unknown model parameters and the estimation method.

2.5.1 Parameter Estimation

The unknown model parameters to be estimated from the inspection data are: the inspectors standard deviations $\sigma_V(I_i)$, the standard deviation of the transition model error σ_W , the transformation function parameter n and the initial state parameters $\{\sigma_0^x, \sigma_0^{\ddot{x}}, p_1, p_2\}$. The parameters are grouped in the following set:

$$\boldsymbol{\theta} = \left\{ \underbrace{\sigma_V(I_1), \sigma_V(I_2), \dots, \sigma_V(I_I)}_{\text{Inspector std.}}, \underbrace{\sigma_W, n}_{\text{Transform. Param.}}, \underbrace{\sigma_0^x, \sigma_0^{\ddot{x}}, p_1, p_2}_{\text{Initial state.}} \right\}. \quad (9)$$

The parameter estimation framework for the parameters $\boldsymbol{\theta}$ is based on the *maximum likelihood estimate* (MLE) method. The MLE estimate is obtained through maximizing the joint prior probability of observations while assuming the observations to be conditionally independent given the state x . Thus, the likelihood for a sequence of observations can be obtained through the product,

$$f(y_{1:T}|\boldsymbol{\theta}) = \prod_{t=1}^T f(y_t|y_{1:t-1}, \boldsymbol{\theta}). \quad (10)$$

In order to avoid numerical instabilities, the natural logarithm is taken for the likelihood estimate. Hence, Equation 10 becomes the *log-likelihood* estimate described by,

$$\ln f(y_{1:T}|\boldsymbol{\theta}) = \sum_{t=1}^T \ln f(y_t|y_{1:t-1}, \boldsymbol{\theta}). \quad (11)$$

Because the analysis in the proposed framework are performed on a network scale, the *log-likelihood* estimate is taken for the inspection sequences of all the structural elements $e_k^j \forall j, k$ combined. Therefore, the network-scale *log-likelihood* becomes,

$$\mathcal{L}(\boldsymbol{\theta}) = \sum_{j=1}^B \sum_{k=1}^{E_j} \sum_{t=1}^{T_k} \ln f(y_{t,k}^j|y_{1:t-1,k}^j, \boldsymbol{\theta}), \quad (12)$$

whereby B is the total number of bridges, E_j is the total number of structural elements in the j -th bridge and T_k is the total number of observations for the k -th structural element. From Equation 12, in order to identify the set of parameters $\boldsymbol{\theta}^*$ that maximizes the *log-likelihood* estimate, the following

optimization problem is to be solved,

$$\begin{aligned}
 \boldsymbol{\theta}^* &= \arg \max_{\boldsymbol{\theta}} \quad \mathcal{L}(\boldsymbol{\theta}), \\
 \text{subject to:} \quad &\sigma_W, \sigma_0^x, \sigma_0^{\ddot{x}} > 0, \\
 &p_1, p_2 > 0, \\
 &\sigma_V(I_i) > 0, \forall I_i \in \mathcal{I}, \\
 &n \in \{1, 2, 3, 4, 5\}.
 \end{aligned} \tag{13}$$

Solving this optimization problem is achieved through an iterative gradient-based optimization framework. The framework is illustrated in the pseudocode shown in Appendix 1. In this framework, the model parameters $\boldsymbol{\theta}$ are optimized initially with the assumption that the standard deviation σ_V of the observation uncertainty is equal across all inspectors, $\sigma_V(I_1) = \sigma_V(I_2) = \dots = \sigma_V(I_{\mathcal{I}}) = \sigma_V$. Therefore, the initial optimization step is performed on the set of parameters $\boldsymbol{\theta}^s = \{\sigma_W, \sigma_V, \sigma_0^x, \sigma_0^{\ddot{x}}, p_1, p_2\}$. This step provides an initial value for the model parameters along with an initial value for the standard deviation associated with each inspector $\sigma_V(I_{1:\mathcal{I}}) = \sigma_V$. Thereafter, the optimization algorithm iterates over the $\sigma_V(I_i)$ parameters while keeping the rest of the model parameters in $\boldsymbol{\theta}$ fixed. The framework keeps iterating over the inspectors parameters $\sigma_V(I_i)$ until the improvements in the objective function $\mathcal{L}(\cdot)$ are less than the tolerance threshold ϵ or the stall limit is met. The stall limit is a predefined number of iterations where improvements in the objective function $\mathcal{L}(\cdot)$ are less than 5%. Following the convergence of the parameters $\sigma_V(I_i)$, the optimization algorithm revisits the model parameters in the subset $\boldsymbol{\theta}^m = \{\sigma_W, \sigma_0^x, \sigma_0^{\ddot{x}}, p_1, p_2\} \subset \boldsymbol{\theta}$. The iterative framework keeps alternating between the $\sigma_V(I_i)$ parameters and the parameters in the subset $\boldsymbol{\theta}^m$ until the global convergence criteria is met. As for the parameter n , since the number of possible values for n is limited, the full optimization procedure is repeated with different n values in order to identify the value that maximizes the objective function. In this optimization scheme, the upper and lower bounds for the model parameters are defined as follows: $\sigma_W \in [10^{-3}, 0.01]$, $\sigma_V \in [1, 10]$, $\sigma_0^x \in [1, 10]$, $\sigma_0^{\ddot{x}} \in [10^{-3}, 0.05]$, $p_1 \in [0, 0.05]$, $p_2 \in [0, 0.15]$. The aforementioned bounds were obtained from experimentation with real and synthetic inspection data in order to ensure the deterioration model is consistent with realistic structural deterioration curves.

3 Data Description

This section presents the datasets employed for verifying and validating the performance of the proposed deterioration model.

3.1 Visual Inspection Data

This dataset includes information from a network of approximately $B \approx 10000$ bridges $\mathcal{B} = \{b_1, b_2, \dots, b_B\}$, located in the province of Quebec, Canada. Visual inspections in this dataset are performed on a yearly scale with dates ranging from late 2007 up to early 2019. During that time-window, the majority of bridges have been inspected from 3 to 5 times. Each structural element e_k^j is evaluated according to a codified procedure [23]. The evaluation method requires the inspectors to break down the evaluation into four categories according to the damage severity. The categories are: A: *Nothing to little*, B: *Medium*, C: *Important* and D: *Very Important*. An example of a structural element inspection data at a given time t is: $y_a = 80\%$, $y_b = 20\%$, $y_c = 0\%$, $y_d = 0\%$. In the example, the inspection data implies that 80% of the structural element area has no damages (category A), while the remaining 20% of the element area has medium damages (category B). Accordingly, the sum of the values under each category (A, B, C, and D) for a single element must be equal to 100% (i.e. $y_a + y_b + y_c + y_d = 100\%$), and the evaluation in each category must pertain to $0\% \leq y_a, y_b, y_c, y_d \leq 100\%$.

3.1.1 Data Preprocessing

Representing the deterioration level using four interdependent metrics increases the complexity of the analysis. This is because of the need to model the deterioration according to each metric while

accounting for the dependency across other metrics. Therefore, data aggregation is applied to transform the four metrics of any inspection point into a single metric. The data aggregation method is similar in concept to the expected utility theory approach [28], where the utilities ω_i are assigned to each state category. Hence, the aggregation formula for any inspection data is,

$$\tilde{y} = \omega_1 y_a + \omega_2 y_b + \omega_3 y_c + \omega_4 y_d, \quad (14)$$

whereby \tilde{y} is the aggregated observation representing the inspection data (y_a, y_b, y_c, y_d) . In this study, the values proposed for the utilities are: $\omega_1 = 1$, $\omega_2 = 0.75$, $\omega_3 = 0.5$, $\omega_4 = 0.25$. Employing the aforementioned utility values restrain the aggregated measure within the range $\tilde{y} \in [25, 100]$. Hence, a structural element with $(\tilde{y} = 100)$ corresponds to the state undamaged $(y_a = 100\%, y_b = 0\%, y_c = 0\%, y_d = 0\%)$, while a structural element with $(\tilde{y} = 25)$ corresponds to the state *Very Important* damage $(y_a = 0\%, y_b = 0\%, y_c = 0\%, y_d = 100\%)$. All numerical analysis are carried out using the aggregated observation \tilde{y} .

3.2 Synthetic Visual Inspection Data

A synthetic dataset is generated to be quantitatively and qualitatively representative of the real inspection database. The total number of structural elements e_k^j in the synthetic dataset is $\mathbf{E} = 10827$. The structural elements considered in this analysis are for the element type *beam*, with an average lifespan of $T = 60$ years. The health condition of the structural elements is represented by a continuous numerical value within the range $\tilde{y} \in [25, 100]$.

To start generating the synthetic data, the true state of deterioration is generated for each synthetic structural element e_k^j through the transition model in Equation 6. The generated true state of the deterioration is ensured to match the qualitative characteristics of a real deterioration by passing through several criteria. These criteria are obtained through empirical experiments and analyses with real and synthetic data. The criteria are,

- a) Slow deterioration: $x_{\frac{T}{2}} > 0.85 \times x_1$.
- b) Plateau in the deterioration curve: $x_T > 0.5 \times x_1$.
- c) Speed threshold: $\dot{x}_1 < 0.01 \times x_1 - 1.3$.
- d) Acceleration threshold: $\ddot{x}_1 < 0.001 \times x_1 - 0.13$.

A deterioration curve with any of the above-mentioned conditions is rejected and excluded from the synthetic database.

After generating the true deterioration curves, a set of 194 synthetic inspectors $\mathcal{I} = \{I_1, I_2, \dots, I_{I=194}\}$ is generated. Each synthetic inspector is assumed to have a zero-mean error with $v_t : V \sim \mathcal{N}(0, \sigma_V^2(I_i))$. The standard deviation $\sigma_V(I_i)$ is generated for each synthetic inspector from a uniform distribution $\sigma_V(I_i) \sim U(\lambda_1, \lambda_2)$. The parameters considered in this study are $\lambda_1 = 1$ and $\lambda_2 = 6$ representing the minimum and maximum values of a uniform distribution. Thereafter, the observation model described in Equation 7 is utilized to generate an observation sample from the true deterioration state. Moreover, in the real dataset, the majority of structural elements has a time series with 3 to 5 observations $\mathbf{y}_{t,k}^j$, while few structural elements have 6 or 8 inspections. This property is also accommodated in the synthetic dataset through weighted sampling. The true state and the observations are generated in the transformed space with a transformation function parameter $n = 3$. The standard deviation of the process error is assumed to be $\sigma_W = 5 \times 10^{-3}$.

4 Deterioration Model Analyses

This section presents the analyses performed using the proposed deterioration framework using synthetic as well as real inspection data.

4.1 Model Verification & Analyses with Synthetic Data

The main goal of performing analysis with synthetic data is to verify the predictive capacity of the proposed deterioration model with a dataset that is representative of the real dataset. The use of synthetic data can also enable verifying the performance of the parameter estimation framework since the model parameters are known in the synthetic case. Estimating the model parameters based on the synthetic data is done as described in Section 2.5.1. The set of model parameters θ estimated through the parameter estimation framework is shown in Table 1, while Figure 4 shows the estimation results of the $\sigma_V(I_i)$ parameters. In Figure 4, the dashed line corresponds to σ_V , which is the initial estimate

Table 1: Estimated model parameters from synthetic inspection data.

σ_W	σ_0^x	σ_V	σ_0^x	p_1	p_2	n
2.1×10^{-3}	1.241	3.001	0.0498	0.0421	0.0611	3

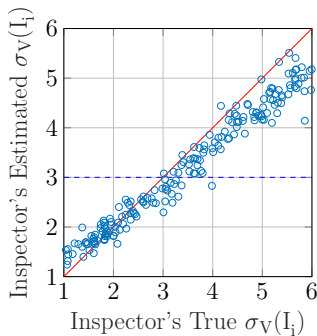


Figure 4: Scatter plot of inspectors true $\sigma_V(I_i)$ vs. estimated $\sigma_V(I_i)$ with a dashed line representing the initial value at the start of the optimization.

for all $\sigma_V(I_i)$, $\forall I_i \in \mathcal{I}$. By considering the alignment among the true and estimated $\sigma_V(I_i)$, the scatter plot in Figure 4 confirms that the proposed parameter estimation method is capable of estimating the inspectors uncertainties $\sigma_V(I_i)$ from network-scale inspection data.

Following the assessment of the estimated model parameters θ^* , the performance of the deterioration model is examined at the structural element level for time series. Examples that demonstrate the predictive capacity of the deterioration model for structural elements are shown in Figures 5, 6 and 7. These examples demonstrate the deterioration model performance for different cases, verified by the true deterioration for the synthetic structural element. The deterioration forecast in the examples is considered for a period of 10 years. The first example shows a low variability case represented by the set of observations $\tilde{\mathbf{y}}_{t,1}^{837}$ from the synthetic structural element e_1^{837} . The deterioration model performance in this example is illustrated in Figure 5, where it can be noticed that the model estimates are consistent with the true deterioration during the prediction phase and stays consistent throughout the total forecast period. The good performance in this case can be attributed to having inspectors with relatively small uncertainties along with consistent inspection data. The speed estimates associated with this case are shown in Figure 6a, in which the speed estimate starts with a low uncertainty when the deterioration speed is near zero due to the model constraints, thereafter, the uncertainty grows larger as the deterioration speed increases. The true deterioration speed, in this case, nearly overlaps with the model estimate throughout the forecast period which demonstrates an excellent forecast performance.

The second example illustrates the deterioration model performance with a series of inspections that has high variability. This case is demonstrated by the set of observations $\mathbf{y}_{t,1}^{792}$ of synthetic structural element e_1^{792} . The model performance in forecasting the deterioration condition is shown in Figure 7. The three observations in this time series came from inspectors that have high uncertainties. This justifies the deviation of the deterioration model from the true state in the prediction phase. In addition, this case emphasizes the importance of estimating the inspectors uncertainties $\sigma_V(I_i)$, given

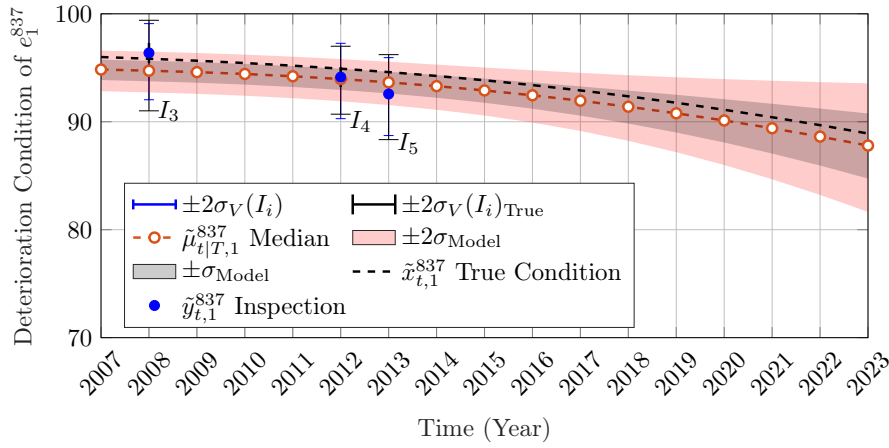
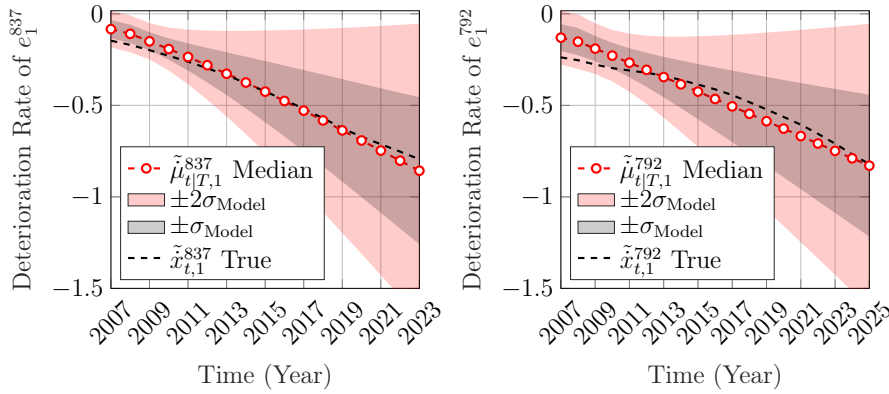


Figure 5: Condition deterioration analysis based on the observations $\tilde{y}_{t,1}^{837} \in [25, 100]$ of the synthetic structural element e_1^{837} with error bars representing the inspectors true (wide whiskers) & estimated (narrow whiskers) uncertainties.



(a) Deterioration speed estimate for e_1^{837} . (b) Deterioration speed estimate for e_1^{792} .

Figure 6: Deterioration speed estimate for synthetic structural elements.

that the model estimate puts more weight on the data from the inspector I_2 because he has a lower uncertainty. The deterioration speed estimate along with the true speed are shown in Figure 6b. The deterioration-speed estimates, as shown in Figure 6b, shows a similar performance to the deterioration condition prediction phase with the true speed being within the $\pm 2\sigma_{\text{Model}}$ interval. It can be noticed that the poor initial speed estimate is associated with an inferior model performance in estimating the deterioration condition. This asserts the importance of having a good initial state estimate for the deterioration model especially in short time-series data.

In order to examine the overall performance of the deterioration model, a test dataset of $E_s = 3250$ ($\approx 30\%$ of E) structural elements e_k^j are analyzed. The deterioration forecast is assessed for a period of 10 years for each structural element $e_k^j \in \mathcal{E}$. The yearly average of the forecast absolute error in the expected condition $\mu_{t|T,k}^j$, the expected speed $\dot{\mu}_{t|T,k}^j$ and the expected acceleration $\ddot{\mu}_{t|T,k}^j$ are shown in Figure 8. In this graph, it can be noticed that the yearly average of the absolute errors in each category increases over the forecast time except for the acceleration; because the condition and the speed are changing monotonically, the errors can accumulate during the forecast; however, the acceleration is locally constant over time so that the errors has the possibility to average out. Moreover, the bias in the expected condition of the forecast is examined with scatter plots generated at different years. The graphs shown in Figure 9 illustrates the true condition $\tilde{x}_{t,k}^j$ versus the model expected condition $\tilde{\mu}_{t|T,k}^j$ generated at forecast years $\{1, 5, 10\}$. It is noticed from Figure 9 that the deterioration model maintains a good predictive capacity over time for the majority of structural elements. Further analysis includes assessing the confidence interval of the model estimates. Specifically,

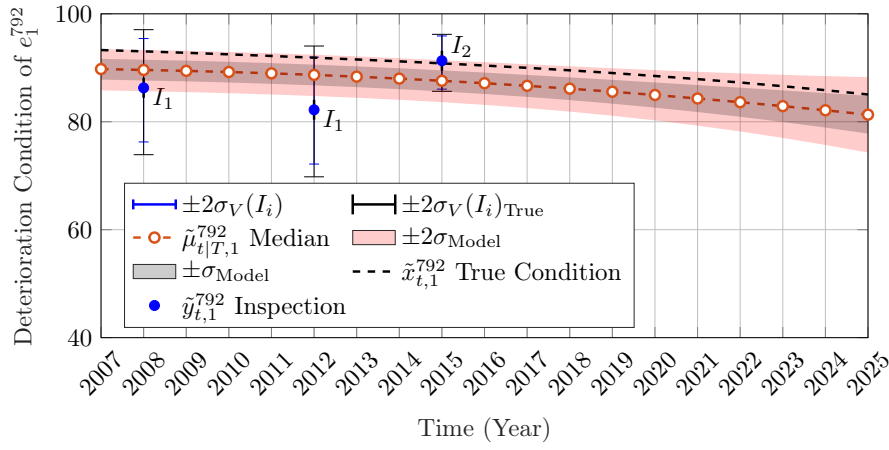


Figure 7: Condition deterioration analysis based on the observations $\tilde{y}_{t,1}^{792} \in [25, 100]$ of the synthetic structural element e_1^{792} with error bars representing the Inspectors true (wide whiskers) & estimated (narrow whiskers) uncertainties.

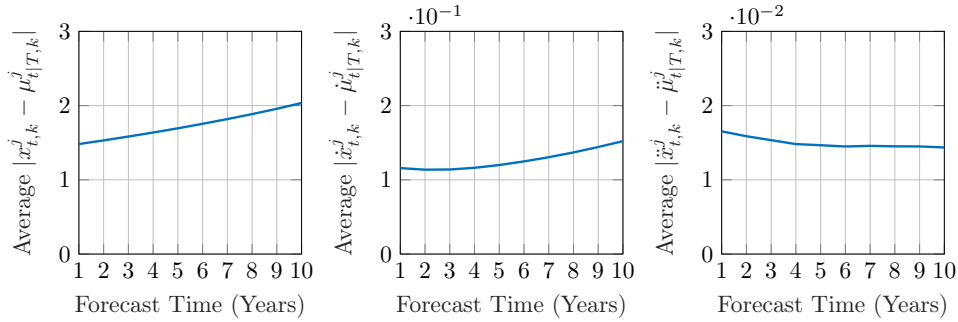


Figure 8: Absolute average error in forecast time for the expected condition, speed and acceleration based on the true condition, speed and acceleration respectively.

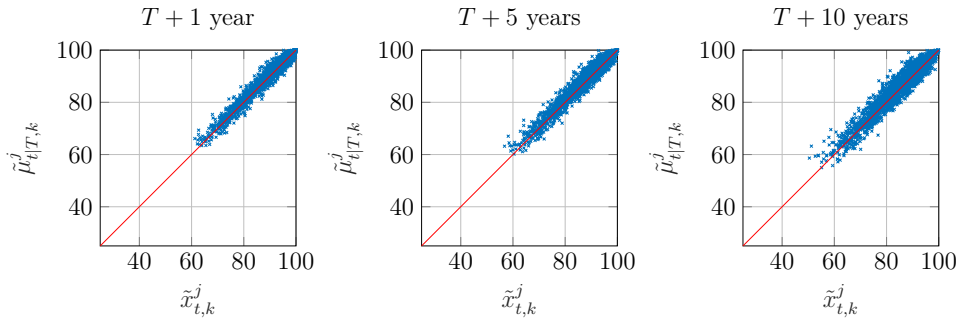


Figure 9: Scatter plot for the model estimate of the condition $\tilde{\mu}_{t|T,k}^j$ vs. the true condition $\tilde{x}_{t,k}^j$ at forecast years 1, 5 and 10.

the probability of the true deterioration condition being within the 95% confidence interval (i.e. $\mu \pm 2\sigma$) of the model state estimate. For that end, the probability of the true state being within the range of $\mu_{t|T,k}^j \pm 2\sigma_{t|T,k}^{x,j}$ is computed at each year and for all structural elements e_k^j . Figure 10 illustrates the aforementioned probability of the model state estimate over the forecast time. In Figure 10, the dashed line represents the average probability of $x_{t,k}^j$ being within $\mu_{t|T,k}^j \pm 2\sigma_{t|T,k}^j$ for a deterioration model with true parameters (including the true initial speed and acceleration for each time series) while the solid line represents the average probability of $x_{t,k}^j$ being within $\mu_{t|T,k}^j \pm 2\sigma_{t|T,k}^j$ for a deterioration model with estimated parameters. It can be noticed that the model with the estimated parameters achieves a probability of $\approx 87\%$ when forecasting one year ahead, while the same model with the true

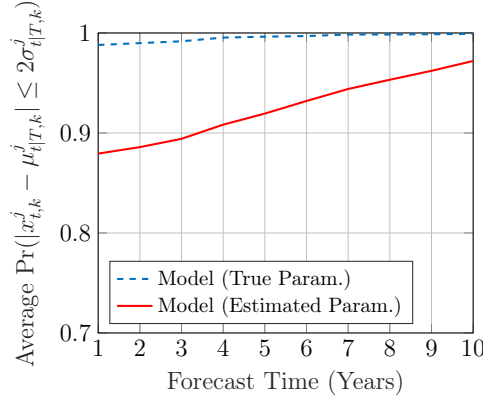


Figure 10: The probability of the true condition being within the 95% confidence interval of the model predicted state for the model with the true parameters (dashed) and the estimated parameters.

parameters has a probability of $\approx 98\%$.

4.2 Model Validation & Analyses with Real Data

Following the verification step, the proposed deterioration model is validated using real inspection data. The dataset considered in the analyses is the inspection dataset for structural elements of type *Beam* taken from bridges $\mathcal{B} = \{b_1, b_2, \dots, b_j\}$. The total number of structural elements employed in the estimation is $\mathbf{E} = 10827$ structural elements representing a sample of 2593 bridges. The majority of the selected structural elements has 3 to 5 inspections per element, performed by different inspectors (a total of 194 inspectors). In this dataset, the health condition of the structural elements is represented by a continuous numerical value within the range $\tilde{y} \in [25, 100]$. It should be noted that the number of structural elements is obtained after excluding time series data that is identified as excessively noisy or insufficient. In this study, an excessively noisy or insufficient time series of a structural element is identified by:

- a) The total number of observations in the time series is less than three.
- b) The number of observations that indicate significant improvement $y_{t+\Delta t} - y_t > 5$ in the structural element is greater than the number of observations indicating otherwise. Δt here refers to the time span between two consecutive observations.
- c) The time series has excessively high observation errors $|y_{t+\Delta t} - y_t| > 15$.

The parameter estimation results for the deterioration model are shown in Table 2 except for the estimated $\sigma_V(I_i)$ values which are represented in a histogram shown in Figure 11. In order to validate

Table 2: Estimated model parameters from real inspection data.

σ_W	σ_0^x	σ_V	$\sigma_0^{\ddot{x}}$	p_1	p_2	n
5.236×10^{-3}	1	4.021	0.049	0.045	0.002	4

the deterioration model performance, different examples for patterns of inspection data are analyzed. The first example for the real inspection data considers the model performance in the case where the set of inspections has a low variability. This case is illustrated in the inspection data shown in Figure 12 for structural element e_1^{14} in bridge b_{14} . In Figure 12, the model estimate has a small uncertainty in the prediction phase. This is attributed to the structural element e_1^{14} being in a near perfect condition according to the inspection data as well as having consistency and low uncertainty in the inspection data. It can be noticed that inspector I_{20} appears to have two different $\sigma_V(I_i)$ showing in the first and the second inspection points. This is because the uncertainty associated with each observation is dependent on the structural element deterioration state $x_{t,k}^j$ as previously detailed in Section 2.3.2. Moreover, the inspection data point at year 2017 (represented by the asterisk symbol) is a validation

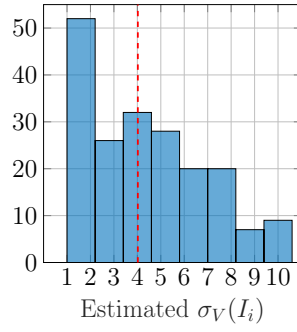


Figure 11: Histogram for the estimated $\sigma_V(I_i)$ values in the transformed space for real inspectors (total: 194 inspectors) with a dashed line representing the initial value at the start of the optimization.

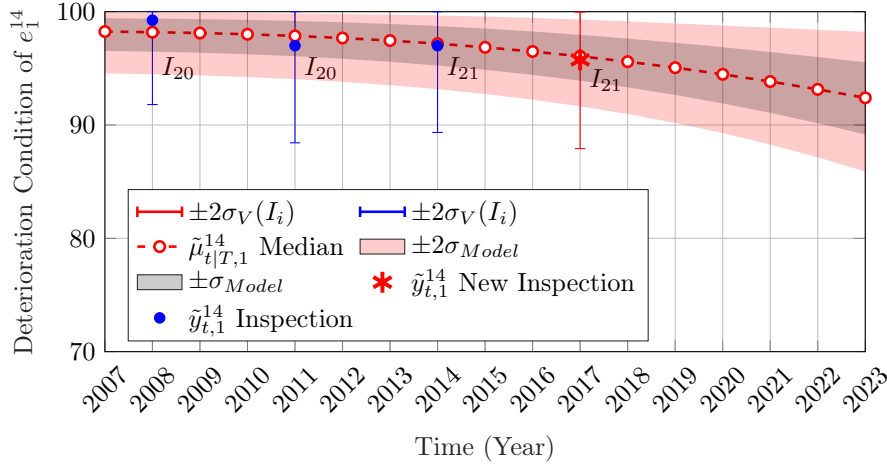
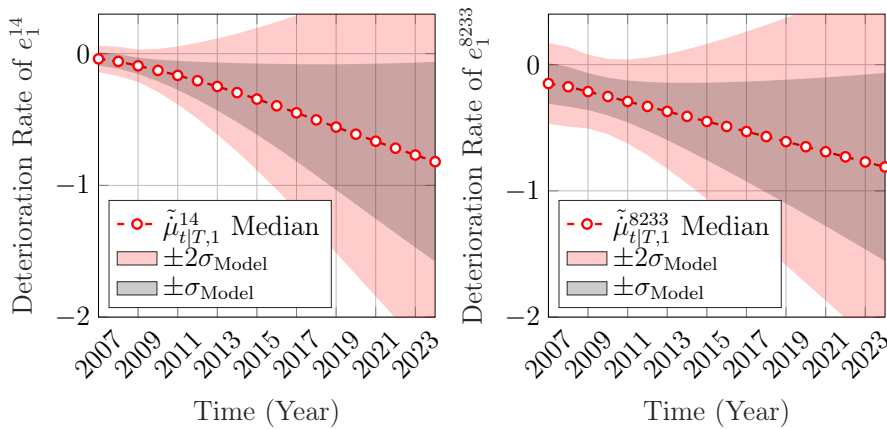


Figure 12: Condition deterioration analysis based on observations $\tilde{y}_{t,1}^{14} \in [25, 100]$ of the real structural element e_1^{14} with error bars representing the inspectors estimated uncertainties.

point which was not included when estimating the model parameters θ^* . It can be noticed that the deterioration model forecast is consistent with this new inspection data. The deterioration speed associated with this condition estimate is shown in Figure 13a.

The next example, shown in Figure 14, demonstrates the model performance in the case where the



(a) Deterioration speed estimate for e_1^{14} . (b) Deterioration speed estimate for e_1^{8233} .

Figure 13: Deterioration speed estimate for real structural elements.

inspection data display high variability. The deterioration model in this case maintains a downward deterioration curve while accounting for the inspections data according to their respective estimated

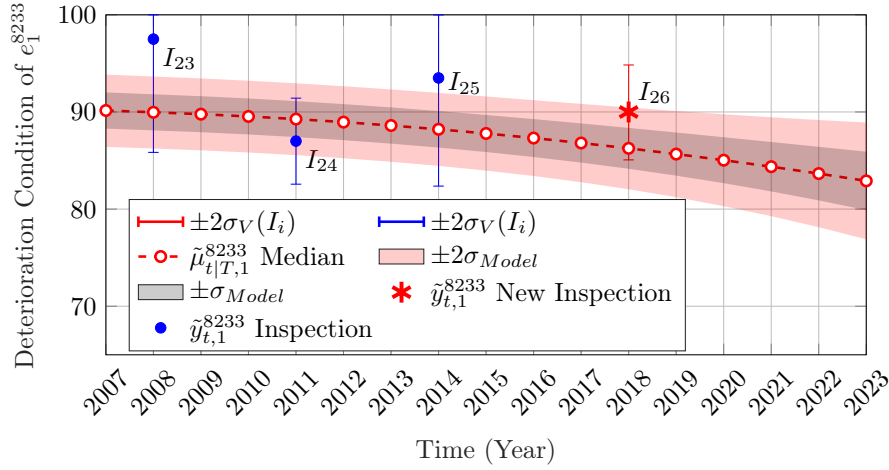
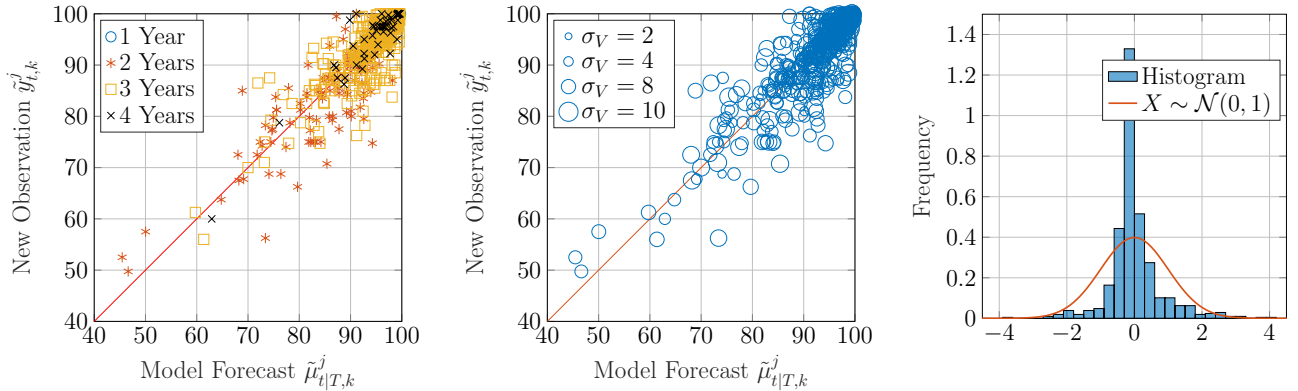


Figure 14: Condition deterioration analysis based on observations $\tilde{y}_{t,1}^{8233} \in [25, 100]$ of the real structural element e_1^{8233} with error bars representing the inspectors estimated uncertainties.

uncertainties. Moreover, and similarly to the previous example, the model forecast stays consistent with the new inspection data point at year 2018. The deterioration speed associated with the condition estimate for e_1^{8233} is shown in Figure 13b.

In order to assess the bias in the deterioration model for the real database, a scatter plot for the model forecast versus new inspection data points is presented in Figure 15a. The term "new inspections" refers to observations that were never used in training the deterioration model. Each point in Figure 15a represent a model forecast $\tilde{\mu}_{t|T}^j$ versus a new inspection \tilde{y}_t^j at time t for a population of structural elements e_k^j . The symbol associated with each point represents the number of years until the new inspection data (observation) has arrived. For example, in a structural element e_k^j , a duration of 4 years refers to the time between two consecutive inspections, in which one of them is the new inspection point. It is worth mentioning that the model forecast is not required to perfectly match the observations



(a) Model forecast $\tilde{\mu}_{t|T,k}^j$ vs. new observations $\tilde{y}_{t,k}^j$ with different symbols representing different forecast durations. (b) Model forecast $\tilde{\mu}_{t|T,k}^j$ vs. new observations $\tilde{y}_{t,k}^j$ with different symbol sizes representing the different uncertainty associated with each observation. (c) Normalized histogram for $(\mu_{t|T} - y_t)/\sigma$ (Transformed Space).

Figure 15: Deterioration condition validation for real structural elements.

due to the presence of observations uncertainties. Considering the same scatter plot, the uncertainty associated with each new observation can be illustrated by the symbol size as shown in Figure 15b. In Figure 15b, the points with the lowest uncertainty are the closest to the diagonal, however, for points with the uncertainty $\sigma_V > 4$, the scatter tend to spread away from the diagonal. Furthermore, it can be noticed that the model does not show any significant sign of bias toward overestimating or underestimating the deterioration condition. In order to further assess the bias, a normalized

histogram is shown in Figure 15c in order to examine the difference between the model forecast and the new observations. The histogram shows that the normalized bias and dispersion in the deterioration model forecast are compatible with the standard Normal distribution. From the analyses above, the deterioration model have displayed a performance similar to the analyses with the synthetic inspection data. This validates the conclusions taken from the analyses with the synthetic data.

5 Conclusion

In this study, a continuous-state deterioration model for visual inspections of bridge-network is proposed. This model enables quantifying the uncertainty of visual inspections through estimating the standard deviation associated with each inspector as well as considering the inspection uncertainty dependent on the deterioration state. The analyses with synthetic data have demonstrated a good performance for the model in estimating the uncertainty associated with each inspector (a total of 194 inspectors). In addition, the deterioration analyses with the synthetic data have shown a good predictive capacity for the proposed framework. The assessment considered a forecast period of 10 years for each synthetic structural element. From the analyses, the probability of the true condition being within the confidence interval $\mu \pm 2\sigma$ of the model forecast is estimated at 87%. The deterioration model has been also validated with real inspection data. The analyses included validation with inspection data that were not included at the model parameter estimation phase. The assessment have shown that the model is unbiased towards overestimating or underestimating the structural elements condition. Overall, the deterioration analyses have shown that the proposed framework has a consistent and robust performance with respect to highly noisy data. Future improvements to the proposed framework can include examining the inspectors bias as well as a Bayesian framework for the estimation of the model parameters. Including the inspector bias can be done through estimating the mean parameter in the observations error term. Furthermore, the analyses with the deterioration speed and acceleration have shown that further improvements on the model are required. Specifically, improving the initial state estimate of the speed and acceleration. This can directly result in improving the model long-term performance. In addition, structural attributes could be factored in the deterioration model to further improve the overall predictive capacity on a network scale.

Acknowledgements

This project is funded by Ministère des Transports du Québec (MTQ). The authors would like to acknowledge the support of René Gagnon for facilitating the access to the inspections database employed in this study.

References

- [1] Duzgun Agdas, Jennifer A Rice, Justin R Martinez, and Ivan R Lasa. Comparison of visual inspection and structural-health monitoring as bridge condition assessment methods. *Journal of Performance of Constructed Facilities*, 30(3):04015049, 2015.
- [2] Yonghui An, Eleni Chatzi, Sung, Han Sim, Simon Laflamme, Bartłomiej Blachowski, and Jinping Ou. Recent progress and future trends on damage identification methods for bridge structures. *Structural Control and Health Monitoring*, 26(10):1545–2255, 2019.
- [3] Yaakov Bar-Shalom, X Rong Li, and Thiagalingam *Estimation with applications to tracking and navigation: theory algorithms and software*. John Wiley Sons, 2004.
- [4] J Bennetts, G Webb, P Vardanega, S Denton, and N Loudon. Quantifying uncertainty in visual inspection data, 2018.
- [5] Leslie E Campbell, Robert J Connor, Julie M Whitehead, and Glenn A Washer. Benchmark for evaluating performance in visual inspection of fatigue cracking in steel bridges. *Journal of Bridge Engineering*, 25(1):04019128

- [6] Pierre Del Moral. Non-linear filtering: interacting particle resolution. *Markov processes and related fields*, 2(4):555–581, 1996.
- [7] Pablo L Durango-Cohen. A time series analysis framework for transportation infrastructure management. *Transportation Research Part B: Methodological*, 41(5):493–505
- [8] Saeed Eftekhari Azam, Ahmed Rageh, and Daniel Linzell. Damage detection in structural systems utilizing artificial neural networks and proper orthogonal decomposition. *Structural Control and Health Monitoring*, 26(2):e2288
- [9] A Ellenberg, A Kotsos, Franklin Moon, and I Bartoli. Bridge related damage quantification using unmanned aerial vehicle imagery. *Structural Control and Health Monitoring*, 23(9):1168–1179
- [10] Charles R Farrar and Keith *Structural health monitoring: a machine learning perspective*. John Wiley Sons, 2012.
- [11] Cláudia Ferreira, Luís Canhoto Neves, José C Matos, and José Maria Sousa Soares. A degradation and maintenance model: Application to portuguese context. *Proceedings of Bridge Maintenance, Safety, Management and Life Extension*, pages 483–489, 2014.
- [12] WR Foster, F Collopy, and LH Ungar. Neural network forecasting of short, noisy time series. *Computers chemical engineering*, 16(4):293–297
- [13] Gongkang Fu and Dinesh Devaraj. *Methodology of Homogeneous and Non-homogeneous Markov Chains for Modelling Bridge Element Deterioration*. Michigan Department of Transportation, 2008.
- [14] Ying-Hua Huang. Artificial neural network model of bridge deterioration. *Journal of Performance of Constructed Facilities*, 24(6):597–602
- [15] Christopher H Jackson. Multi-state models for panel data: the msm package for r. *Journal of statistical software*, 2011.
- [16] Simon J Julier and Jeffrey K Uhlmann. Unscented filtering and nonlinear estimation. *Proceedings of the IEEE*, 92(3):401–422 0018–9219, 2004.
- [17] JD Kalbfleisch and Jerald F Lawless. The analysis of panel data under a markov assumption. *Journal of the American Statistical Association*, 80(392):863–871
- [18] MJ Kallen and JM Van Noordwijk. Statistical inference for markov deterioration models of bridge conditions in the netherlands. In *Proceedings of the Third International Conference on Bridge Maintenance, Safety and Management*, number 16-19, 2006.
- [19] Rudolf Emil Kalman. Contributions to the theory of optimal control. *Bol. Soc. Mat. Mexicana*, 5(2):102–119, 1960.
- [20] Jaeho Lee, Kamalarasa Sanmugarasa, Michael Blumenstein, and Yew-Chaye Loo. Improving the reliability of a bridge management system (bms) using an ann-based backward prediction model (bpm). *Automation in Construction*, 17(6):758–772
- [21] Chi-Jie Lu, Tian-Shyug Lee, and Chih-Chou Chiu. Financial time series forecasting using independent component analysis and support vector regression. *Decision Support Systems*, 47(2): 115–125
- [22] Roman Matkovskyy and Taoufik Bouraoui. Application of neural networks to short time series composite indexes: Evidence from the nonlinear autoregressive with exogenous inputs (narx) model. *Journal of Quantitative Economics*, 2018.
- [23] *Manuel d’Inspection des Structures*. Ministère des Transports, de la Mobilité Durable et de l’Électrification des Transports, Jan 2014.

- [24] Mark Moore, Brent M Phares, Benjamin Graybeal, Dennis Rolander, and Glenn Washer. Reliability of visual inspection for highway bridges, volume i. Technical report, Turner-Fairbank Highway Research Center, 6300 Georgetown Pike, 2001.
- [25] See-King Ng and Fred Moses. Bridge deterioration modeling using semi-markov theory. *A. A. Balkema Uitgevers B. V, Structural Safety and Reliability.*, 1:113–120, 1998.
- [26] Eugene OBrien, Ciaran Carey, and Jennifer Keenahan. Bridge damage detection using ambient traffic and moving force identification. *Structural Control and Health Monitoring*, 22:1396–1407, 2015.
- [27] Goran Puž, Jure Radić, and Irina Stipanovi Oslaković. A new model for stochastic analysis of bridge durability. *Grafëvinar*, 62(04.):287–297 0350–2465, 2010.
- [28] John Quiggin. *Generalized expected utility theory: The rank-dependent model*. Springer Science Business Media, 2012.
- [29] Lawrence R Rabiner. An introduction to hidden markov models. *iee assp magazine*, 3(1):4–16, 1986.
- [30] Herbert E Rauch, CT Striebel, and F Tung. Maximum likelihood estimates of linear dynamic systems. *AIAA journal*, 3(8):1445–1450 0001–1452, 1965.
- [31] Marilyn Ryall. *Bridge management*. CRC Press, 2007.
- [32] Dan Simon. Kalman filtering with state constraints: a survey of linear and nonlinear algorithms. *IET Control Theory Applications*, 4(8):1303–1318
- [33] Dan Simon and Donald L Simon. Constrained kalman filtering via density function truncation for turbofan engine health estimation. *International Journal of Systems Science*, 41(2):159–171
- [34] Jojok Widodo Soetjipto, Tri Joko Wahyu Adi, and Nadjadji Anwar. *Bridge Deterioration Prediction Model Based On Hybrid Markov-System Dynamic*, volume 138. EDP Sciences, 2017.
- [35] Serdar Soyoz and Maria Q Feng. Instantaneous damage detection of bridge structures and experimental verification. *Structural Control and Health Monitoring*, 15(7), 2008.
- [36] HR Noël Van Erp and André D Orcesi. The use of nested sampling for prediction of infrastructure degradation under uncertainty. *Structure and Infrastructure Engineering*, pages 1–11 1573–2479, 2018.
- [37] Emily K Winn. Artificial neural network models for the prediction of bridge deck condition ratings. Master’s thesis, Michigan State University, 2011.
- [38] Ivan Zambon, Anja Vidovic, Alfred Strauss, Jose Matos, and Joao Amado. Comparison of stochastic prediction models based on visual inspections of bridge decks. *Journal of Civil Engineering and Management*, 23(5):553–561, 2017. doi: 10.3846/13923730.2017.1323795.
- [39] Ivan Zambon, Anja Vidović, Alfred Strauss, and Jose Matos. Condition prediction of existing concrete bridges as a combination of visual inspection and analytical models of deterioration. *Applied Sciences*, 9(1):148, 2019.
- [40] Yi Zhang, Chul-Woo Kim, and Kong Fah Tee. Maintenance management of offshore structures using markov process model with random transition probabilities. *Structure and Infrastructure Engineering*, 13(8):1068–1080, 08 2017.

Appendix 1

Algorithm 1 Parameter Estimation Framework

Require: θ_0^s : Initial parameters vector

- 1: $L_1 \leftarrow -10^{10}$ (Initial *log-likelihood*)
- 2: $\epsilon \leftarrow 10^{-3}$ (Convergence tolerance)
- 3: $\rho_1 \leftarrow 10, \rho_2 \leftarrow 10$ (Stall limits)
- 4: $s_1 \leftarrow 1, s_2 \leftarrow 1$ (Initial stall)
- 5: $\nu_1 \leftarrow 300, \nu_2 \leftarrow 1$ (Iteration limit per parameter)
- 6: $\theta_1^s \leftarrow \text{NewtonRaphson}(\mathcal{L}(\theta^s), \theta_0^s, \nu_1)$
- 7: $\sigma_V(I_{1:I}) = \sigma_V, \sigma_V \in \theta_1^s$
- 8: $L_2 \leftarrow \mathcal{L}(\theta_1^s)$
- 9:
- 10: **for** $n := 1$ to 5 **do**
- 11: **while** $|L_{j+1} - L_j| \leq \epsilon$ or $s_1 \geq \rho_1$ **do**
- 12: **while** $|L_{j+1} - L_j| \leq \epsilon$ or $s_2 \geq \rho_2$ **do**
- 13: $L_j \leftarrow L_{j+1}$
- 14: **for** $i := 1$ to I **do**
- 15: $\sigma_V(I_i) \leftarrow \text{NewtonRaphson}(\mathcal{L}(\sigma_V(I_i)), \sigma_V(I_{i0}), \nu_2)$
- 16: $L_{j+1} \leftarrow \mathcal{L}(\sigma_V(I_{1:I}))$
- 17: **if** $|(L_{j+1} - L_j)/L_j| \leq 0.05$ **then**
- 18: $s_2 = s_2 + 1$
- 19: $\theta_{j+1}^m \leftarrow \text{NewtonRaphson}(\mathcal{L}(\theta^m), \theta_j^m, \nu_1)$
- 20: $L_j \leftarrow \mathcal{L}(\theta_{j+1}^m)$
- 21: $s_1 = s_1 + 1$
- 22: **return** θ_{j+1}^m and $\sigma_V(I_{1:I})$ (Resulting parameters)
